12-5-2023

Experimental investigation of temperature polarisation by capturing the temperature profile development over DCMD membranes

Hiras Ahamed Hijaz
Edith Cowan University

Masoumeh Zargar
Edith Cowan University

Abdellah Shafieian
Edith Cowan University

Amir Razmjou

Mehdi Khiadani
Edith Cowan University

10.1016/j.memsci.2023.122089
Hijaz, H. A., Zargar, M., Shafieian, A., Razmjou, A., & Khiadani, M. (2023). Experimental investigation of temperature polarisation by capturing the temperature profile development over DCMD membranes. Journal of Membrane Science, 687, 122089. https://doi.org/10.1016/j.memsci.2023.122089

Journal of Membrane Science 687 (2023) 122089

Contents lists available at ScienceDirect

Journal of Membrane Science

journal homepage: www.elsevier.com/locate/memsci

Experimental investigation of temperature polarisation by capturing the temperature profile development over DCMD membranes

Hiras Ahamed Hijaz [a], Masoumeh Zargar [a], Abdellah Shafieian [a], Amir Razmjou [b], Mehdi Khiadani [a,*]

[a] School of Engineering, Edith Cowan University, 270 Joondalup Drive, Joondalup, Perth, WA, 6027, Australia
[b] UNESCO Centre for Membrane Science and Technology, School of Chemical Engineering, University of New South Wales, Sydney, NSW, 2052, Australia

ARTICLE INFO

Keywords:
Temperature polarisation
Temperature profile
Membrane distillation
Surface temperature

ABSTRACT

Temperature polarisation (TP) is a major drawback limiting the global acceptance of membrane distillation (MD) technology. TP is typically quantified using a dimensionless index known as Temperature Polarisation Coefficient (TPC). TPC has significant limitations, whereby it cannot be used to compare different MD configurations or design conditions, nor to analyse the TP phenomenon along the membrane. In this research, the temperature profile over and along a lengthy DCMD membrane has been measured under various operational conditions, where its impact on TP has been explored for the first time. A specialised DCMD membrane cell was manufactured to capture temperature profiles, both along and over the membrane surfaces, using miniature thermocouples. The effects of flow rate and feed temperature were investigated on the temperature profiles. The results showed that the extent of TP was not constant along the membrane, and that the temperature profile was not symmetrical across the feed and permeate side, predominantly due to the effects of the inlet and outlet on the flow. The TPC value calculated using the conventional method was not able to accurately reflect the TP phenomenon along the membrane, indicating TPC to be an ineffective tool to study TP along the membrane.

1. Introduction

Membrane distillation (MD) has been characterised as an energy-intensive process, one only favoured when used in combination with solar energy or waste heat [1,2]. The main hindrances of the MD process are its: temperature polarisation (TP), concentration polarisation (boundary layers formation), membrane conductivity (heat transfer through conduction of membrane), membrane wetting, scaling and fouling [3]. In MD systems, TP is a key cause of flux reduction. According to Abu Zeid et al. [4], 50–80% of the driving force in the MD process is wasted due to the TP phenomenon. This is because, according to the Antoine Equation (1), the vapour pressure is exponentially related to the temperature. Consequently, any changes in the temperature will have a major impact on the driving force of the system, as illustrated by:

$$P_{pw} = \exp\left(23.237 - \frac{3481.2}{T - 45}\right) \quad (1)$$

where, P_{pw} is the vapour pressure for pure water and T is the temperature in Kelvin.

The effect of TP causes a difference in temperatures between the localised bulk feed and its corresponding membrane surface, which results in the formation of a non-isothermal boundary layer in the vicinity of the hydrophobic membrane. The term *localised bulk* refers to the fact that the bulk temperatures of both feed and permeate will change when the fluid moves along the membrane; hence, producing different 'localised bulk' temperatures along the membrane. For direct contact membrane distillation (DCMD), TP happens at both the feed and permeate sides. At the feed side, the temperature at the membrane surface is lower than that of the bulk feed temperature, due to the cooling effects of evaporation and heat loss resulting from membrane conduction. Accordingly, the membrane surface temperature at the permeate side is higher than its bulk temperature, as the hot water vapour condenses at the vicinity of the membrane surface due to absorbed heat via the membrane. These occurrences reduce the vapour pressure difference across the membrane, thereby significantly reducing the driving force of the MD system [5]. For this reason, membranes with low thermal conductivity are preferred for long membrane modules [6].

* Corresponding author.
E-mail addresses: h.mohamedhijaz@ecu.edu.au (H.A. Hijaz), m.zargar@ecu.edu.au (M. Zargar), a.shafieiandastjerdi@ecu.edu.au (A. Shafieian), amir.razmjou@ecu.edu.au (A. Razmjou), m.khiadani@ecu.edu.au (M. Khiadani).

https://doi.org/10.1016/j.memsci.2023.122089
Received 26 June 2023; Received in revised form 18 August 2023; Accepted 12 September 2023
Available online 14 September 2023

Nomenclature

P_{pw}	Vapour pressure for pure water
T_f	Bulk temperature of feed side
T_p	Bulk temperature of permeate side
T_{if}	Temperature at the membrane interface (surface) of the feed side
T_{ip}	Temperature at the membrane interface (surface) of the permeate side
h_f	Convective heat transfer coefficient of feed solution
h_p	Convective heat transfer coefficient of permeate solution
Re	Reynolds Number
D_h	Hydraulic diameter of the rectangular duct
ν	Kinematic viscosity
V_{avg}	Average flow velocity
TP	Temperature Polarisation
TPC	Temperature Polarisation Coefficient
MD	Membrane Distillation
DCMD	Direct Contact Membrane Distillation
VMD	Vacuum Membrane Distillation
AGMD	Air Gap Membrane Distillation
SGMD	Sweeping Gas Membrane Distillation

In 1987, Schofield [7] introduced a dimensionless parameter, known as Temperature Polarisation Coefficient (TPC), to quantify the effects of TP. They defined TPC for a DCMD module as given in Equation (2),

$$TPC = \frac{T_{if} - T_{ip}}{T_f - T_p} \tag{2}$$

where T_f and T_p are the bulk temperatures of the feed and permeate sides respectively, and T_{if} and T_{ip} are temperatures at the membrane interface (surface) of the feed and permeate sides, respectively. Hence, TPC values can vary between 0 and 1. TPC reaches a value of 0 when the effect of TP is high, and the TP is minimised when the TPC value is close to 1. For DCMD modules, TPC values are commonly in the range of 0.4–0.7 [8]. This definition has been widely accepted by many researchers for the DCMD configuration [5]. Similarly, TPC has been also defined for other MD configurations (i.e., VMD, AGMD, SGMD) [9–14].

Generally, TPC is calculated by measuring bulk temperatures at the inlets, by using external thermocouples [15], and estimating surface membrane temperatures by interpolations and iteration using heat and mass transfer equations [5,16]. However, due to conductive heat losses, it is expected that the temperature drops from the feed inlet to the feed outlet, in addition to temperature increasing from permeate inlet to permeate outlet. Therefore, estimating a single value for surface temperature is inaccurate, especially for a long membrane module. Identifying this imprecision, Manawi et al. [16] have developed a model to predict intermediate temperature along the membrane, as a means to calculate *local* TPC values along the membrane rather than using a single conventional *average* TPC value. They claim that the flux calculations from their model using *localised* TPC are closer to experimental results than the conventional method. Using this predictive model, TP decreased with decreasing the feed temperature, increasing the permeate temperature and increasing flow rate. These findings are compatible with trends found using conventional TPC calculations [17].

Although, in the literature, there are numerous studies that investigate the TP phenomenon using Computational Fluid Dynamics (CFD) [18–20], only a few studies [21–23] have investigated the TP phenomenon by estimating surface temperature empirically. To study the *local* TP phenomenon along the MD module experimentally, Tamburini et al. [21] have used a non-invasive technique combining colour-changing crystals (Thermochromic Liquid Crystals (TLCs)) and digital image analysis [21]. The experimental setup did not include a real membrane, where rather, the membrane properties were carefully simulated using TLC sheets and a polycarbonate layer. Applying this technique, they were able to investigate the variation of surface temperature along the membrane, local TPC and local heat transfer coefficients. The best geometrical features for spacers were determined accordingly. Santoro et al. [22] used two optical techniques to monitor the temperature of the membrane surface and the bulk temperature. PVDF Electrospun nanofibrous membranes were doped with $Ru(phen)_3$ in order to monitor surface temperature changes along the membrane. The bulk temperature variation was monitored using an IR camera. The bi-dimensional maps of membrane surface temperatures for both feed and permeate sides were plotted accordingly. Within their experiment, they observed that the *bulk* temperatures of both feed and permeate across the inlet and outlet were only varied by approximately 2 °C. However, the change in surface temperatures along the membrane was considerably greater, by multiple folds. It is worth noting here, that only results for one operating condition were reported in this research, where no comparison between different operating conditions against surface temperature or local TPC was determined.

TPC has also been quantitatively evaluated by Ali et al. [23], using 16 thermocouples located at specific locations. At the feed side, four thermocouples were positioned at the membrane surface along the membrane, and the other four thermocouples were used to measure the localised bulk temperature. This arrangement was duplicated at the permeated side with the remaining 8 thermocouples. Although measurements were made at 4 locations in the study to determine local TPCs, local TPC variation along the membrane was ignored in the analysis, while 'average TPC' values were reported. The authors concluded that the average TPC increases with increasing *Re* number.

Within the literature to date, the majority of research studies have applied the conventional TPC definition to analyse the TP phenomenon, even though the global definition of TPC is known to be inadequate. Surprisingly, there is a lack of attention in the literature deviating from the dependency on TPC values when studying the TP phenomenon. This research proposes a unique method for experimentally building a temperature profile perpendicular to the membrane, to move away from the dependency on TPC values to study the TP phenomenon. Highly sensitive and accurate miniature thermocouples are placed near the membrane surface (0.3 mm) to measure temperature along the membrane for both feed and permeate sides. The temperature difference across membrane is a good indicator of the magnitude of the driving force for water production. This research quantifies the TP phenomenon by analysing the temperature difference between the measured *localised bulk* and respective surface temperatures. Unlike most studies in the literature that have estimated an overall TPC for MD systems, this research will analyse the TP phenomenon along the membrane. Additionally, this paper will study how temperature profile, i.e., the TP phenomenon, will behave when the flow rate is increased, as increasing the flow rate is the most common technique used to mitigate TP [5]. The feed temperature, one of the important operating parameters that influences the permeate flux of MD systems, will be also investigated against the temperature boundary layer formation. The effects of other operating conditions (i.e., feed salinity, permeate temperature and flow orientation) will be investigated in our future studies.

Studying temperature profiles and their behaviour, with varying operating conditions, will give in-depth knowledge of TP behaviour. This study could help in developing better techniques to mitigate TP effectively and economically. As TP is one of the key limitations of MD systems, its mitigation is an essential step in the global acceptance of MD systems. Accordingly, the results of this study can help navigate the future trajectory of scientific and commercial studies on MD systems. The results obtained can be utilised for choosing the optimised designing and operating parameters that minimise the TP phenomenon for the effective design and operation of future DCMD cells.

2. Experimental setup

The general layout of the overall DCMD setup is shown in Fig. 1. A membrane module with a high membrane length-to-width ratio was manufactured to investigate the TP phenomenon along the membrane. (Fig. 2). The feed and permeate compartments were built using polycarbonate sheets, as they withstand high temperatures and have transparent properties. A commercial PTFE membrane (*Memsift Innovation Singapore,* Table 1) with active surface area of 0.026 m^2 (650 mm × 40 mm) was sandwiched between the feed and permeate compartment. No mechanical support was used. as the application of mechanical support has been reported to interfere with the surface temperature of membranes in DCMDs [16,24]. The overall height of the feed/permeate compartment was 7 mm.

Two recirculating heater/chiller (Across International, 10–99 °C.) were used to circulate the feed and permeate water, and to maintain their inlet temperatures accordingly. The flow rates and inlet bulk temperatures on both sides were measured by two compact magnetic flowmeters (SM6020, IFM), as shown in Fig. 1. The magnetic flowmeters were used, as they provide the least resistance to the flow. SM6020s can read low flow rates from 0.05 ± 0.02 L/min, while temperatures within the range of -20—90 °C ± 0.1 °C can be measured. To measure the outlet temperature, mineral-insulated thermocouples (k-type) with a measurable continuous temperature range of 0–1100 °C were used. The recirculating heater, also used as the feed tank, was placed on a mass scale (*Adam GFK 75H*), with a minimum readability of 1 g, to record the loss of feed mass during operation. Mass scale measurements were data logged in real-time every minute. In addition, the salinity of the feed was fixed at a brackish water level (i.e., 3 g/L) before the commencement of each experiment.

The temperature readings to generate temperature boundary layer were measured at points *A, B, C* and *D* along the centre of the membrane, as shown in Fig. 3. Six miniature thermocouples of 0.5 mm diameter (*TC Measurement & Control,* −185 to +300 ± 0.1 °C*)* were grouped at each point to generate the temperature profile and the readings were recorded by a temperature data logger (Fig. 1). The disturbance caused locally by the miniature thermocouples is negligible compared to the active membrane area. The thermocouples were arranged in an oval shape (Fig. 3), and care was taken to maximize the separation between each thermocouple. Ample distance was maintained between each point, namely A, B, C, and D, to ensure that the disturbances caused by adjustable points were negligible. The temperature data logger (Lutron BTM-4208SD) was set to record the temperature every second.

The closest thermocouple to the membrane surface was placed 0.3

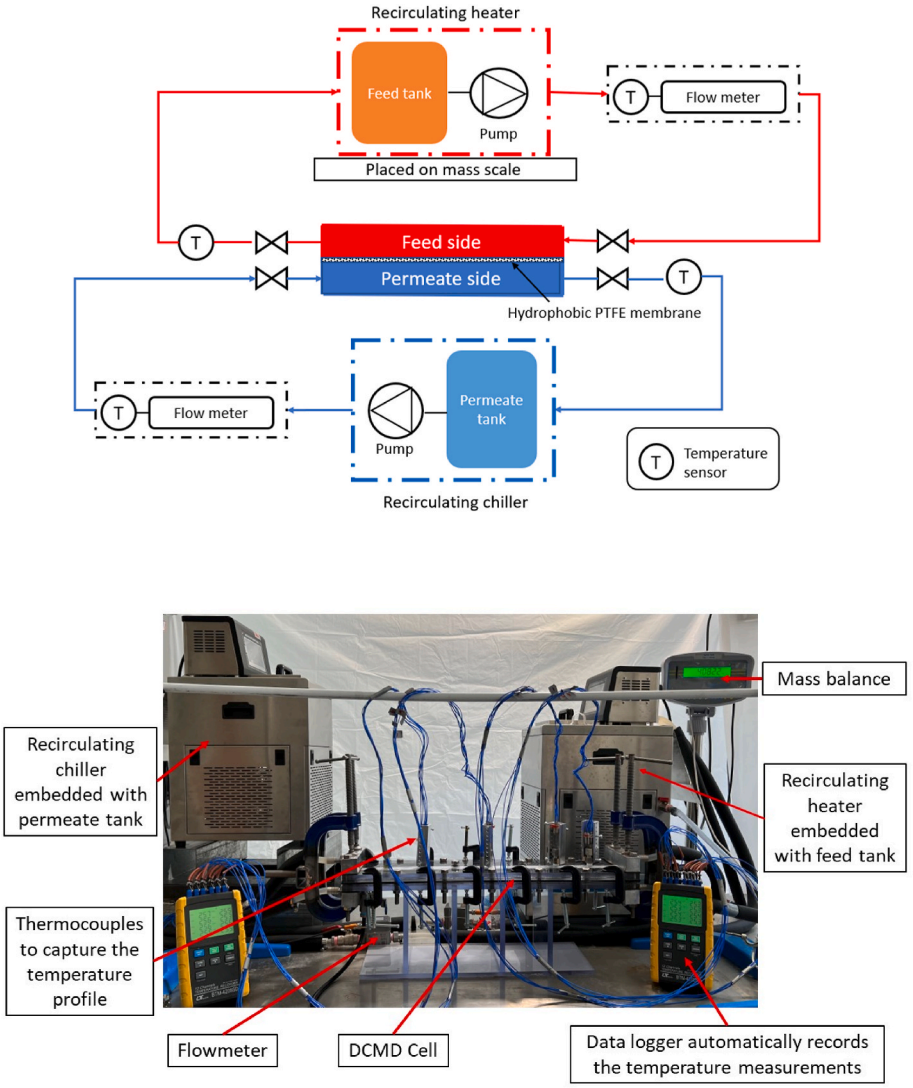

Fig. 1. Overall schematic layout of the DCMD experimental setup (top). The feed cycle is represented with red lines and permeate cycle is represented with blue lines. The picture of the established DCMD setup (bottom). The thermocouples attached measure the temperature profile at different points along the membrane cell. (For interpretation of the references to colour in this figure legend, the reader is referred to the Web version of this article.)

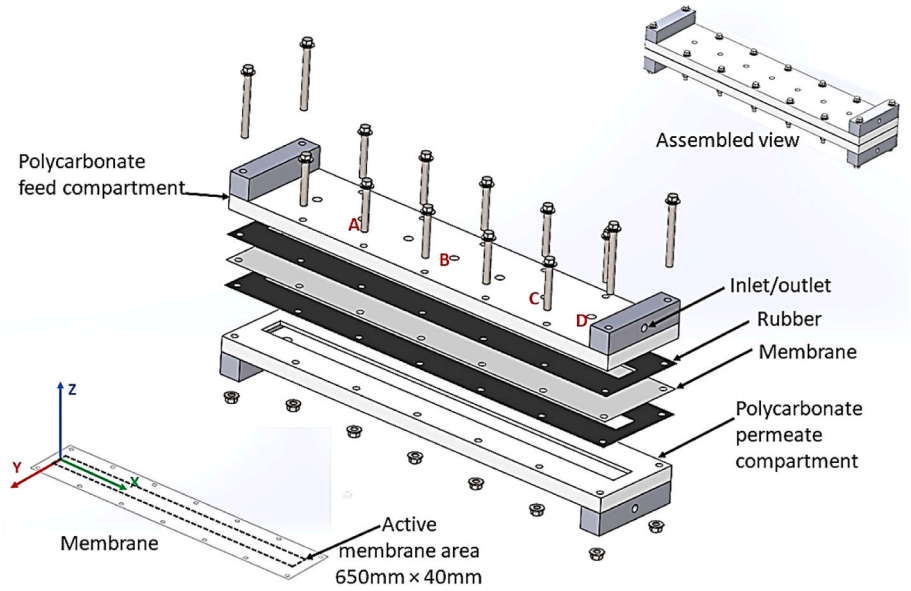

Fig. 2. DCMD cell specially designed for this experiment with the feed and permeate compartment sandwiching the hydrophobic PTFE membrane. Assembled view of the DCMD cell (top right). In the global coordinate system used in this paper, the origin is placed on the membrane (bottom left).

Table 1
Membrane properties as provided by the commercial supplier (Memsift Innovation).

Item	Parameter	Unit
Membrane material	PTFE	–
Support layer	PET	–
Average pore size	0.22	μm
Average thickness	150	μm
Contact angle	130 ± 4	deg
Liquid entry pressure of water (LEPw)	>300	kPa
Max-continuous operating temperature	80 ± 1	°C

mm away from the membrane at each point. The next five thermocouples were placed consecutively at 0.25–1.5 mm away from each other, after which their exact distance from the membrane surface was recorded (Fig. 3). The intent was to place the thermocouples closer to the membrane in order to accurately capture critical temperature changes and to avoid interference from the feed/permeate compartment wall. The positioning of the six thermocouples of each set was not the same for all four points of A, B, C and D due to practical difficulties. At each point (A, B, C and D), the set of six thermocouples was passed through a thermocouple position holder (Fig. 3), consisting of a sealant, a follower, and a vacuum sealant, which served to hold the thermocouples in position and prevent any leakages. Due to their thin diameter (0.5 mm) and complex path, the thermocouples were prone to slight bending and movement, making it extremely difficult to replicate the exact positioning to any other set of six thermocouples. As the goal of the research was to capture the temperature profile at each point A-D, the vertical distance from the membrane was normalized to facilitate comparison of results.

Temperature readings were measured initially at the feed side, after which the experiments were repeated to take measurements from the permeate side. As the membrane did not have any mechanical support (to avoid interference with sensitive temperature readings), the feed and permeate flow rates were kept the same for each operating condition, in order to minimise membrane warping and to prevent the membrane from moving from its original position. Typically, in the literature, the feed flow rate or the permeate flow rate has been varied while the other flow rate is kept constant. However, due to the high sensitivity of this system to the relative position of thermocouples to the membrane, both flow rates were varied at once, and kept the same for varying flow rates experiments.

Before any measurements were recorded, the system was allowed ample time to stabilise. The experiments were then conducted for 40 min. All the experiments were carried out under counter current mode, meaning that point *A* (X/L = 0.24) (Fig. 3a) was closest to the feed inlet and furthest to the permeate inlet.

Table 2 summarises the operating conditions used in this paper. The first set of experiments was carried out for varying flow rates of feed and permeate. The feed and permeate temperatures were fixed at 55 °C and 25 °C, respectively. A feed salinity of 3 g/L NaCl was used for all experiments. The flow rates varied from 0.3 L/min to 2.8 L/min with a 0.5 L/min variation. The lower critical Reynolds number (laminar to transient flow) was considered as 2000 and the higher critical Reynolds number (transient to turbulent flow) is considered as 4000 [25]. Based on this definition, this research speculated the overall flow condition (whether it was laminar, transient or turbulent). However due, to the close proximity of the flow inlets and outlets, the flow conditions (laminar, transient or turbulent) may vary along the membrane. Future research could investigate the local variations in flow velocity along the membrane.

The flow channel is considered as a rectangular duct with a width and height of 40 mm and 7 mm, respectively. The Reynolds number (Re) is calculated using equation (3) and presented in Table 3 [25].

$$Re = \frac{V_{avg} * D_h}{v} \tag{3}$$

where D_h is the hydraulic diameter of the rectangular duct, v is the kinematic viscosity [26] and V_{avg} is the average velocity.

The second set of experiments was carried out for varying feed temperatures. From the first set of experiments, it was evident that choosing a flow rate with a low *Re* number was the best option to analyse the TP phenomenon with varying feed temperatures (Section 3.7). Hence, a flow rate of 0.5 L/min was fixed at both the feed and permeate sides of the module. The permeate temperature and feed salinity were fixed at 25 °C and 3 g/L, respectively. The feed temperature was varied from 35 °C to 75 °C, with an increment of 10 °C. Accordingly, each experiment has been labelled as feed temperature (°C)_permeate temperature (°C)_flow rate (L/min). For example, 55 °C_25 °C_0.8 L/min represents a feed temperature of 55 °C, permeate temperature of 25 °C

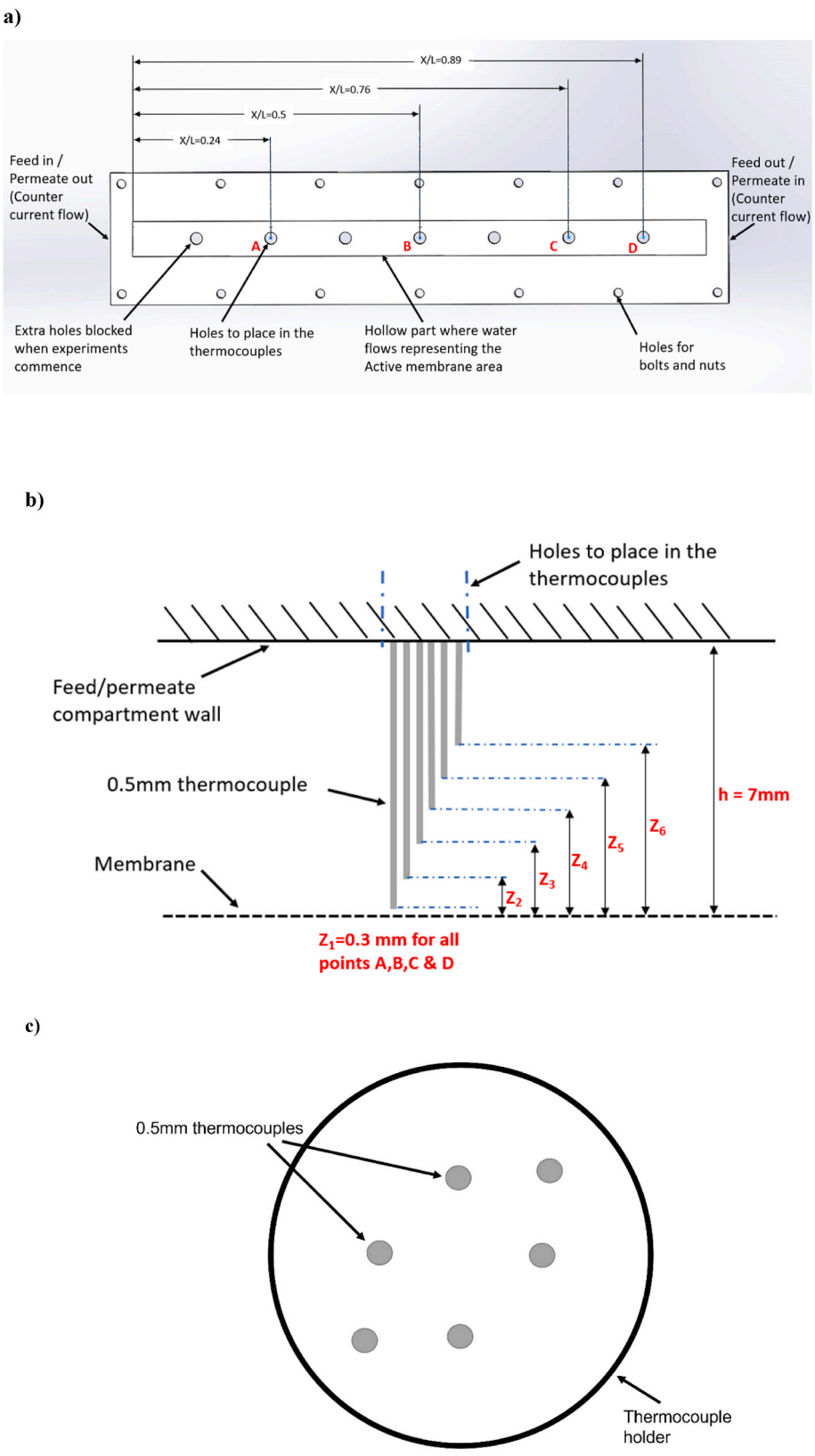

Fig. 3. **a**) Inner top view of Feed/Permeate compartments with relative dimensions along the membrane (top) and **b**) a representation of how the thermocouples are arranged perpendicular to the membrane (middle)) c) bottom view of the thermocouple holder showing the arrangement of the six thermocouples at each point (A,B, C or D) (bottom).

Table 2
Operating conditions applied. The first set of experiments was carried for varying flow rates (0.3–2.8 L/min) and the second set of experiments for varying feed temperature (35 °C–75 °C).

Parameters	Feed temperature (°C)	Permeate temperature (°C)	Salinity (g/L NaCl)	Flow rate (L/min)
1st set of experiments	55	25	3	0.3 to 2.8 with 0.5 L/min increments
2nd set of experiments	35 to 75 with 10 °C increments	25	3	0.5

Table 3
The Reynolds number calculated for the feed and permeate sides for the first and second sets of experiments. The flowrates at feed and permeate sides were kept equal for each experiment.

First set of experiments: varying flow rates. (Constant parameters: feed temperature = 55 °C, permeate temperature = 25 °C and salinity = 3 g/L)						
Varying flow rates (L/min)	0.3	0.8	1.3	1.8	2.3	2.8
Re number (Feed side	414	1104	1794	2484	3174	3864
Re number (Permeate side)	236	629	1022	1415	1808	2200
Second set of experiments: varying feed temperature. (Constant parameters: permeate temperature = 25 °C, flow rates = 0.5 L/min and salinity = 3 g/L)						
Varying feed temperature (°C)	**35**	**45**	**55**	**65**	**75**	
Re number (Feed side)	486	585	690	799	911	
Re number (Permeate side)	393	393	393	393	393	

and a flow rate of 0.8 L/min at both sides of the membrane.

3. Results and discussion

3.1. Temperature profiles along the membrane

Fig. 4 shows the average temperature recorded perpendicular to the membrane for different positions along the membrane for the operating conditions of 55 °C_25 °C _0.8 L/min. According to the coordinate system (Fig. 2), Z/H represents the relative positioning perpendicular to the membrane, while X/L represents the relative positioning along the membrane (L = 650 mm and H = 7 mm). In this paper, the terminologies *along* and *across* the membrane are used concerning the x-axis and z-axis, respectively. The temperature difference between the closest and furthest points to the membrane (Z/H) represents the extent of the TP. Accordingly, the higher the difference, the greater the TP effect. The gradient of the graph represents the rate at which the temperature changes, whereby the steeper the slope, the higher the polarising effects in that region.

At the *feed* side, the temperature of the feed solution is the lowest closest to the membrane surface. This is because of the cooling effects of evaporation when the water vapour moves across the membrane from the feed side to the permeate side. For all points (*A, B, C* and *D*), the majority of the polarisation happens closest to the membrane surface (Z/H < 0.4). The steepness of the gradient lowers away from this point (Z/H > 0.4), where the temperature asymptotes towards the localised bulk value. One of the ways to mitigate the effects of TP is to increase the convective heat transfer coefficient(s) (h_f and h_p) by enhancing the turbulence and mixing of the solution [5]. Point *A* experiences the highest disturbance/mixing due to the inlet effect of the flow, which enhances convective heat transfer (also referred to in section 3.7). Therefore, Point *A* (X/L = 0.24) has the lowest TP effects, as this is closest to the feed inlet. Midway in the channel (Point *B*), the TP becomes more significant than at Point *A*, while Point *C* has the highest TP effects. Points *C* and *D* have a much similar temperature profile patterns. However, it was observed in some other experiments with different operating conditions that Point *C* had a slightly higher TP than Point *D* (Figs. 12 and 13). This is because Point *D* is the closest measured point to the feed outlet, whereby the outlet effects on the feed flow affect the temperature profile.

The average temperature decreases when moving from Points *A* to *C* at the *feed* side. This may be due to heat losses by membrane conduction as the TP effects increase along the membrane. The temperature profile is not substantially developed, whereby TP is not significant at Point *A*. Then, the temperature profile develops along the membrane, whereby the TP effects become more dominant. Observing the temperature profile development, it can be speculated that the temperature profile development along the membrane behaves similarly to the temperature profile development for a hot fluid moving along a cold flat surface. The temperature profile slowly develops along the fluid flow path until it fully develops at a specific point along the flat surface [27,28]. However, these two occurrences are different in concept because in MD systems

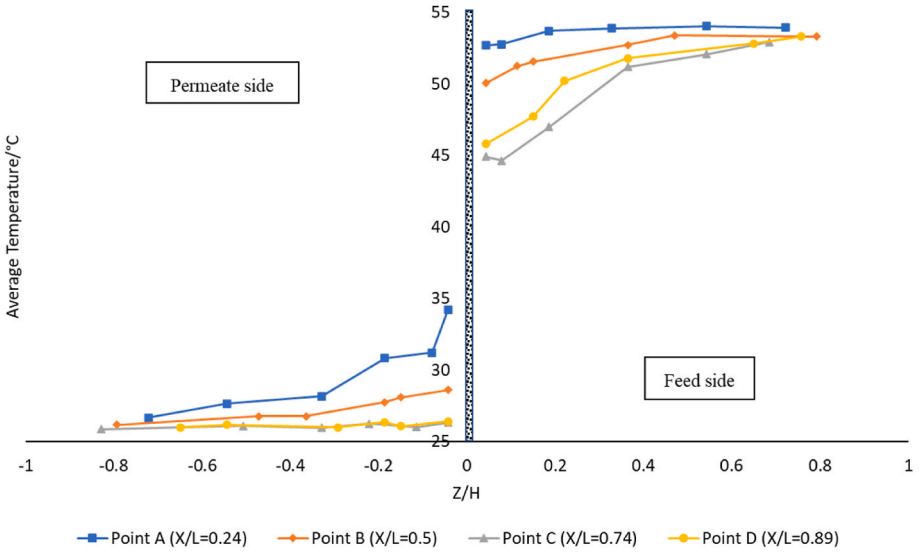

Fig. 4. The average temperature recorded for 55 °C _25 °C _0.8 L/min at different locations along the membrane for a counterflow operation. Point A is closest to the feed inlet, point B is the midpoint and point D is closest to permeate inlet.

mass transfer occurs through the membrane. Points *C* and *D* have very similar profiles, where it appears that the temperature profile has fully developed at Point *C*. However, it is difficult to conclude that the temperature profile has been fully developed at Point *C*, as the feed outlet might also influence the temperature profile at Point *D*. Therefore, it would be interesting to examine how the profiles would behave with longer membrane modules and without the influence of the outlets.

According to a numerical study [6] on long membrane modules, for a module length of 5000 mm at the feed side, their result shows, closer to the inlet (length <500 mm) the difference between the surface temperature and bulk temperature increases. Then, for a given module length (500 mm–1500 mm), the temperature difference between the surface and bulk remains almost constant and then the temperature difference starts reducing (length >1500 mm). This is consistent with the results obtained along the membrane in this research. The temperature difference between the surface temperature and localised bulk increases (From Point A to C) closer to the inlet and then remains nearly constant (From Point C to D). In this research, the declination of the temperature difference was not observed as the module used is smaller in size (L = 650 mm). However, Ali et al. [6] had a different trend in the permeate side compared to the feed side. In their study, at the permeate side, the surface and bulk temperature differences remain constant and minimal, and no development of temperature profile was projected. Additionally, the rate of temperature drops along the membrane for both the surface and bulk decreased when the module length was increased (5000 mm, 10 000 mm and 20 000 mm module lengths), though, the exit temperature were almost the same, under same operating conditions. Accordingly, when the MD module length increases the overall TP decreases. In the same research, Ali et al. [6] states that, in relation to the process performance, the feed velocity is the strong operating condition that determines the optimum module length. Feed temperature and membrane thickness also are vital parameters when determining the optimum module length.

At the *permeate* side, the same trend can be observed but from the opposite direction, as this system operates in counterflow mode. Point *A* has maximum temperature profile development as it is the furthest point from the permeate inlet. Another reason for this development is that at Point *A* of the feed side, the surface temperature (T_{if}) is the highest recorded, which induces a higher polarisation at the permeate side. Points *C* and *D* have almost the same temperature profiles and the least TP effect, as they are closest to the permeate inlet. The similarity in the temperature profiles of Points *C* and *D* are more profound at the permeate side than at the feed side. This indicates that the effect of inlet on the TP development is more impactful than the effect of the outlet. Further, same as the feed side, the highest impact of TP (Z/H < −0.4) occurs closest to the membrane.

3.2. Effect of flow rates on the temperature profile

In this section, the focus is on the behaviour of the temperature profiles along the membrane for varying flow rates. As noted earlier, the flow rate of both the feed and permeate sides were kept equal for each experiment. The feed and permeate temperatures were fixed at 55 °C and 25 °C, respectively.

Fig. 5 shows that the temperature difference between the *localised bulk* and respective surface temperatures decreased when the flow rate increased for all points along the membrane. This proves that the TP is minimised when the *Re* number increases. When the *Re* number is increased, the turbulence activities are increased, whereby there is higher mixing in the vicinity of the membrane surface. This creates better convective heat transfer, which results in the temperature at the membrane surface moving closer to the localised bulk temperature [29, 30].

Temperature polarisation is sensitive at low *Re* numbers, whereby any variation in the flow rate at a low *Re* number results in a significant change in the temperature profile. The temperature profile experienced the most significant impact when the flow rate was changed from 0.3 L/min to 0.8 L/min, as depicted in Fig. 5. This alteration exerted a greater influence on the temperature distribution compared to other variations in flow rate. This indicates that changes in flow rates have a more notable impact on temperature distribution in the initial stages of laminar flow. Further to this, Ali et al. [23] have identified these

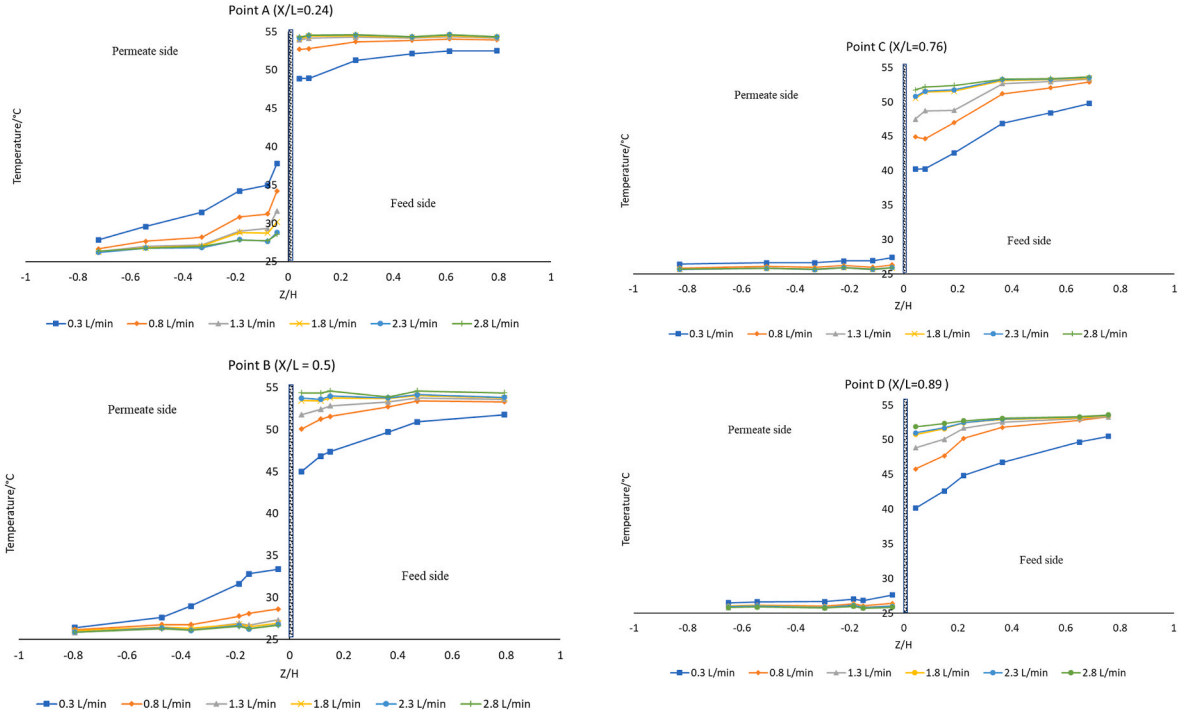

Fig. 5. Average temperature readings at points A, B, C and D for varying flow rates ranging from 0.3 L/min to 2.8 L/min. The feed and permeate temperatures are fixed at 55 and 25 °C, respectively and the salinity at 3 g/L.

sensitivities using TPC calculations where TPC had steeper gradients against *Re* at low *Re* numbers. However, Manawi et al. [16] have reported a linear relationship between the *Re* and TPC values.

Besides this, for all cases of different flow rates, the effects of the inlet and outlet also influenced the temperature profile along the membrane for both the feed and permeate sides, as discussed in the previous section (Section 3.1). When the flow rate approaches the turbulent region (i.e., flow rates >2.3 L/min) the TP was least significant and was negligible at Points *C* and *D* at the permeate side. Therefore, when designing a DCMD module, it is not a bad assumption to neglect the TP effects for smaller membrane modules (<15 cm) operating in the turbulent mode. Shafieian et al. [31] have also recommended that flow rate should be operated near/at the turbulent region for higher water productivity.

3.3. Surface temperature along the membrane for varying flow rate

The closest thermocouple was placed 0.3 mm away from the membrane surface, where measurements from the closest thermocouple are considered as the surface temperature in this research. The surface temperature for different points along the membrane for varying flow rates is shown in Fig. 6. Along the flow direction, the surface temperature decreased at the feed side and the surface temperature increased at the permeate side. This is because of the cooling effects of evaporation and heat losses due to membrane conduction as explained in Section 3.1. There is almost a linear change in the surface temperature along the membrane from Point *A* to Point *C*. However, Points *C* and *D* have similar surface temperatures due to Point *D* being closer to the feed outlet and the permeate inlet (Section 3.1).

Overall, the feed and permeate sides have similar temperature differences along the membrane, although in all cases the permeate side had a slightly higher temperature difference than the feed side. Between the feed and permeate sides, the highest discrepancy in temperature difference along the membrane was recorded for the flow rate of 0.3 L/min, which was also the maximum temperature difference along the membrane recorded among varying flow rates (Fig. 6). From Point *A* to Point *D* (422 mm apart) the temperature differed by 8.7 °C and 10.1 °C at the feed side and permeate side, respectively.

Residence time is defined as the ratio of the length of the channel to the flow velocity [32]. When the flow rate increases, the residence time shortens. This results in a fixed amount of fluid moving along the membrane in a short time. Consequently, when the flow rate is increased (i.e., decreased residence time) the change in surface temperature along the membrane decreases (Fig. 6). The surface temperature starts close to the inlet temperature for both the feed and permeate sides, and then the change in surface temperature is influenced by the flow rate. When the flow rate gets to near turbulence state, the change in surface temperature is minimal. From the results, it can be inferred that the shorter the membrane modules, the more effective the system is when operated at a low *Re* number.

Experimenting with a flow rate of 0.3 L/min at the feed side (Fig. 6), resulted in the average *surface* temperature dropping to 40.2 °C at Point *C* from the inlet feed temperature of 55 °C. This high change in temperature can be attributed to two reasons: heat loss due to membrane conduction, and temperature profile (TP) development along the membrane. The consequences of both these adverse factors are prevalent at point *C* (X/L = 0.76) resulting in a high change in surface temperature. Similarly, at the permeate side, the average surface temperature at Point *A* increased to 37.8 °C from the inlet permeate temperature of 25 °C. High changes in surface temperatures have also been reported by Santoro et al. [22] for the operating condition of 60 °C_18–19 °C_0.2 L/min. They reported that the surface temperature dropped approximately by 20 °C and 18.4–19.4 °C from their bulk values at the feed and permeate sides, respectively. In both studies, the changes in bulk temperature from the inlet and outlet were lower than the surface temperature along the membrane.

According to a CFD modelling [33], the surface temperatures can be enhanced by reducing the flow compartment height, as the surface temperature approaches the bulk temperatures due to decrease in flow channel. Consequently, the permeate flux increases as the effects of TP are lowered. In future studies, these observations from the simulations can be validated by capturing temperature profiles using thermocouples, as introduced in our study.

3.4. Effect of feed temperature on the temperature profile

This section looks at the effect of feed temperature on the temperature profile and TP. When the feed temperature was increased, the TP is increased for all points (*A, B, C* and *D*) as the temperature difference between the *localised bulk* and respective surface temperatures at that point increases according to Fig. 7. With increasing feed temperature, the temperature difference across the membrane increases, resulting in an enhanced vapour pressure difference (driving force). This consequently increases the permeate flux. As more water vapour is transferred across the membrane, the feed temperature at the vicinity of the feed membrane interface lowers. This is due to the cooling effects of evaporation and the heat loss from the mass transfer. The hot water vapour

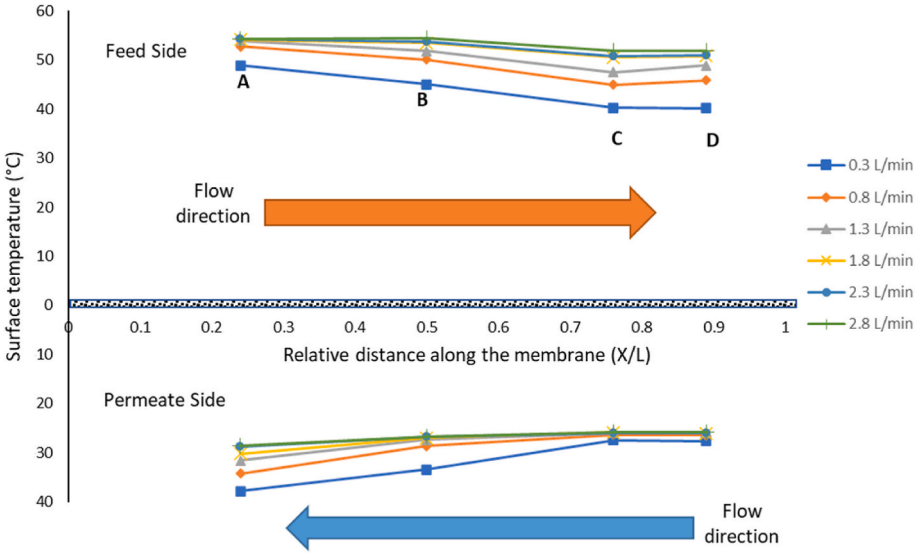

Fig. 6. The surface temperature measured for varying flow rates at the feed side (top) and the permeate side (bottom).

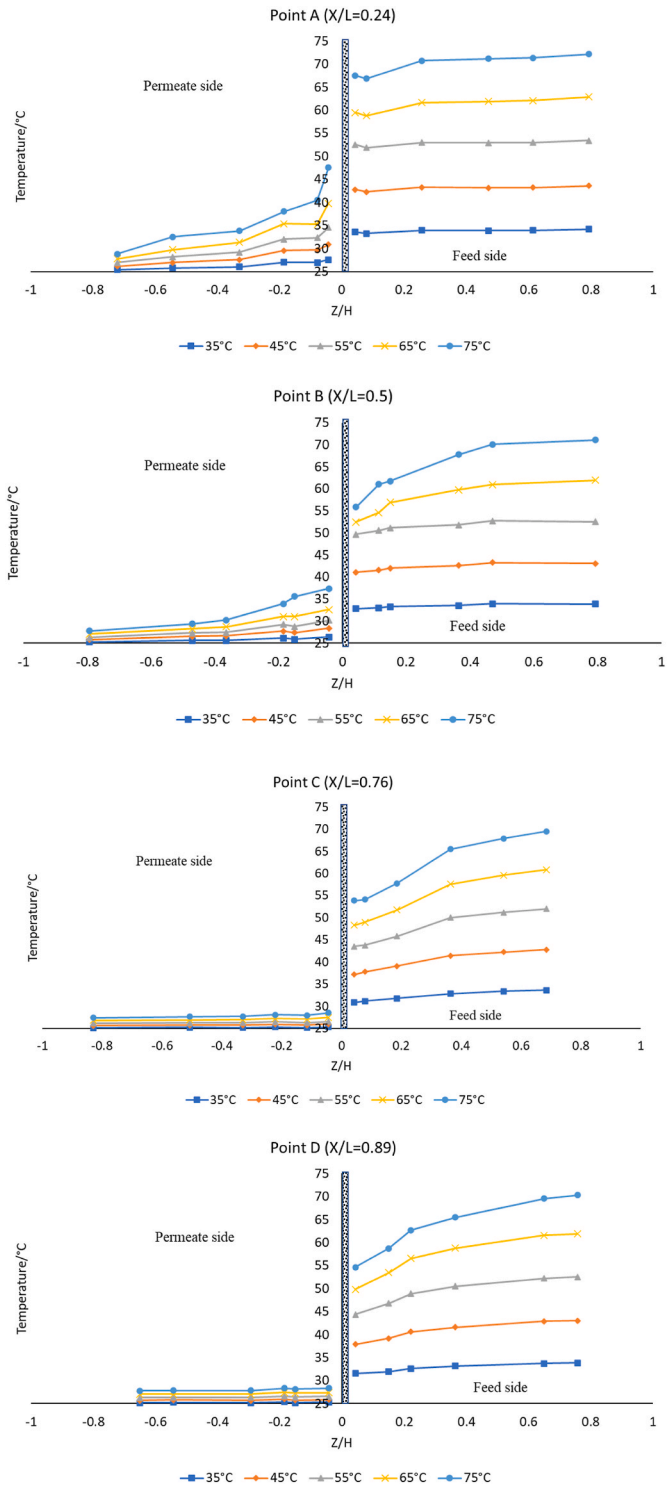

Fig. 7. The average temperature for different points A, B, C & D along the membrane for varying feed temperatures ranging from 35 °C to 75 °C. The permeate temperature, flow rate and salinity were fixed at 25 °C, 0.5 L/min, and 3 g/L respectively.

condenses at the permeate membrane interface, increasing the temperature of the permeate side at the interface of the membrane. Increasing the feed temperature increases TP at both the feed and permeate sides of the membrane [34].

The graphs are all clustered at the *permeate* side as the permeate temperature is fixed at 25 °C for all cases (Fig. 7). However, there is a slight increase in the overall temperature readings when the feed temperature is increased. Temperature polarisation is not significant at Points *C* and *D* on the permeate side, as these points are close to the permeate inlet. The temperature profile becomes more profound when moving away from the permeate inlet. As with the first set of experiments (i.e., varying flow rates), the highest temperature changes across the membrane (Z-axis) occurred closest to the membrane for both permeate and feed sides. At the *feed* side, the TP was not significant at Point *A* except at high feed temperatures (Fig. 7). Along the membrane, the temperature difference between the *localised bulk* and respective surface temperatures increases. Same as with varying flow rates, the temperature profiles at Points *C* and *D* looks almost the same at the feed side. This builds a good argument that the temperature profile has been fully developed for the feed side around Point *C*. However, this observation is not conclusive as the feed outlet might affect the temperature readings at Point *D*, as discussed in Section 3.2.

Khayet et al. [35] have argued in their paper that the polarisation of temperature is not symmetrical for the feed and permeate sides. Figs. 5 and 7 confirm this statement, where the asymmetricity of TP is apparent for various points (*A, C* and *D*) along the membrane. They emphasised that the values for the feed and permeate heat transfer coefficients (h_f and h_p) must be different, as the temperature, type of solution, and hydrodynamic conditions are different. This would result in an asymmetrical polarisation between the feed and permeate. The research showed that the flow direction (counterflow) plays the major role in the asymmetry polarisation phenomena along the membrane. The h_f and h_p at each point along the membrane are dominantly influenced by the proximity of the inlet and outlet of the feed and permeate. Khayet et al. [35] also pointed out that polarisation can be symmetrical at low-temperature differences between inlet feed and permeate temperatures with diluted solutions. Point *B*, the midpoint of the DCMD cell, is the point that is least affected by the influence of flow direction as this DCMD cell is built symmetrically along the membrane. Looking at Point *B* (Fig. 7), it can be inferred that the polarisation is symmetrical for low-temperature differences and the asymmetricity becomes apparent at high-temperature differences. Khayet et al. [35] also concluded that there is higher polarisation at the feed side than at the permeate side. This was observed for all points along the membrane except point *A* in our study which can be due to the mitigation of polarisation at Point *A* on the feed side by the feed inlet. Point *B*, the point least affected by flow direction, supports this conclusion. Although Points *C* and *D* also support this conclusion, this is heavily influenced by the fact that permeate inlet is in proximity to Points *C* and *D*. The results suggest that a system operated under concurrent flow would be under more representative operating conditions to validate the theories of asymmetry in polarisation.

3.5. Impact of feed temperature on the surface temperature

Point *A* has the highest surface temperature for both the feed and permeate sides due to concurrent flow (Fig. 8). This means that at the feed side, Point *A* is the closest to the feed inlet and; hence, close to the inlet feed temperature value. In contrast, at the permeate side, Point *A* is closest to the permeate outlet and the surface temperature increases along the flow direction from the condensing water vapour and membrane conduction. There is a decline in the surface temperature between Points *A* and *C* for the same reasons explained in Section 3.3. As witnessed with the varying flow rates experiments, the surface temperatures for Points *C* and *D* are almost the same.

From Points *A* to *D* (422 mm apart), the feed and permeate sides had similar changes in surface temperature along the membrane for low feed temperatures. At high feed temperatures (65 °C and 75 °C), the discrepancy between the feed and permeate increased for surface temperature changes along the membrane. At the inlet feed temperature of 75 °C, the temperature difference along the feed (from point *A* to *D*) is 12.9 °C. This occurred, however, at 19.2 °C at the permeate side. Unlike the first set of experiments with varying flow rates where the

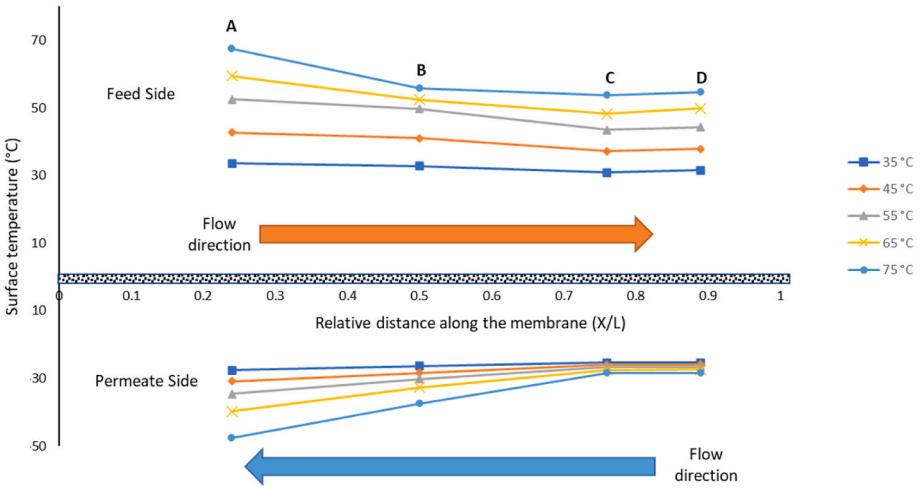

Fig. 8. the surface temperature at different points along the membrane with increasing feed temperatures of 35 °C, 45 °C,55 °C,65 °C & 75 °C, for the feed side (top) and permeate side (bottom).

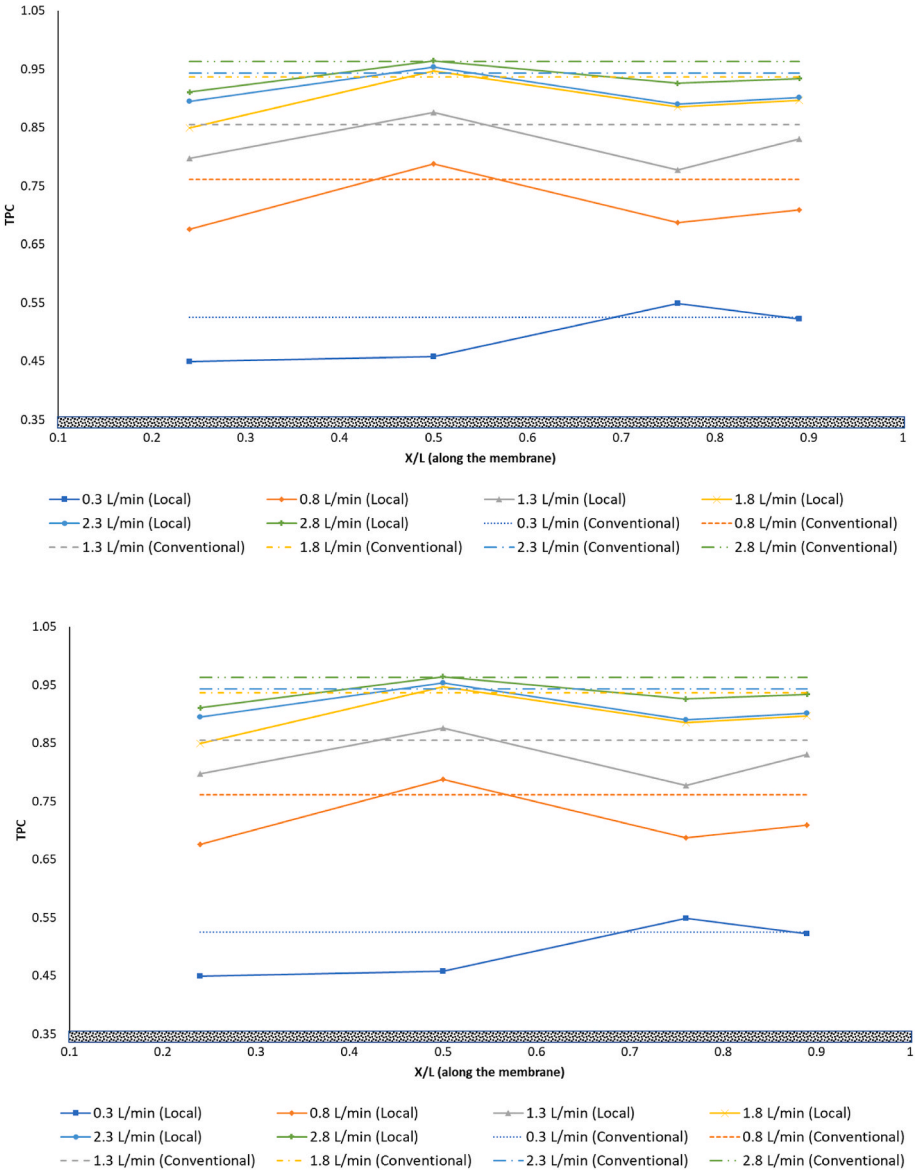

Fig. 9. TPC calculations using the conventional method and localised values for varying flow rates (top) and varying feed temperatures (bottom).

discrepancy between feed and permeate surface temperature across the membrane was minute, here, the discrepancy is significant. This conflicts with the model prediction from the works of Manawi et al. [24], where they estimated the change in surface temperature to be equal for both feed and permeate sides when operated at a feed and permeate temperature of 70 °C and 20 °C (high inlet temperature difference), respectively for a flow rate of 1.5 L/min.

3.6. A comparison between conventional TPC value and localised TPC values for varying flow rate and feed temperature

Typically, in the literature, for conventional TPC calculations a single value is calculated, neglecting the temperature variation along the membrane. The calculation generally uses *measured* inlet temperatures as 'bulk' temperatures [15] and *estimated* surface temperature by iteration and interpolation [5,16]. In this research, as the surface temperatures have been experimentally measured at four points along the membrane, an *average* measured surface temperature is used in the calculation of conventional TPC value (equation (1)) (Fig. 9). As the general practice, the bulk temperature values are obtained by measuring the inlet and outlet temperatures in this research. When the membrane modules are longer, (as in this research compared to other laboratory setups), it is wise to use the definition used by Manawi et al. [16], where they defined the 'bulk' temperature as the average of the inlet and outlet bulk temperatures. The bulk TPC value was calculated using this definition. The results were compared with *localised* TPC values along the membrane using the technique used by Ali et al. [23]. These authors measured the local surface and *localised* bulk temperatures to calculate the local TPC values at 4 points along the membrane. However, in their case, they reported the findings as an averaged TPC value rather than local TPC values along the membrane.

It is evident from Fig. 9 that the TPC calculations are not an appropriate tool to investigate the TP phenomenon along the membrane, especially when the system is operated under the counterflow mode. This is because two opposing trends are witnessed in the feed and permeate sides along the x-axis of the membrane. These trends influence the TPC values along the membrane. It would be interesting to investigate how the TPC values will behave when the system is operated in the concurrent flow configuration where the trends might align along the x-axis of the membrane.

Khayet et al. [35] have shown that the TP is asymmetrical at feed and permeate sides; therefore, they introduced separate TPC definitions for feed and permeate sides rather than using an overall for the MD system. This approach is more appropriate than the general TPC definition, especially when the system is operated in counterflow mode. Conversely, Manawi et al. [16] have predicted steady increments in local TPC values along the membrane for a counter current flow setup. The model was divided into 10 elements, and they predicted increments until the last element where there was a sudden drop in TPC value. Prior to the current research, consideration was not given with regard to the temperature profile developed along the membrane, and a similar TP effect was assumed along the membranes. Hence, their predicted model [16] has discrepancies with the experimental local TPC calculated in this research. Distinctive to the linear local TPC values calculated in counterflow mode in their research, Manawi et al. [16] predicted fluctuating local TPC values along the membrane for concurrent flow. However, Santoro et al. [22] reported the local TPC values decreased along the membrane module for a concurrent flow experimental setup.

TPC calculations are a better indicator for studying TP effects with varying flow rates than for analysing along the membrane. Thus, this can be utilised to obtain a quick understanding though it is not feasible for vigorous analysis of TP phenomena. Fig. 9 also shows TP is most sensitive at low *Re* numbers; hence, the difference between the TPC values is greater in the laminar region than in the turbulent region. Ali et al. [23] have witnessed a similar trend though in their case, only the feed flow rate was varied while the permeate flow rate was fixed. Similarly, TPC is only a good indicator for a quick understanding of the TP phenomenon when the feed temperature varies (Fig. 9). At high feed temperature (i.e., high-temperature difference across the membrane), when the TP is high, the TPC varies significantly. However, when the feed temperature is close to the permeate temperature and TP is insubstantial, the TPC values do not change significantly. The TPC values calculated, using the conventional method, for feed temperatures 55 °C, 45 °C and 35 °C are almost identical.

3.7. Further comparison between flow rate and feed temperature variations

Fig. 10a shows that the permeate flux increases with increasing the *Re* number. The flux increases linearly at lower *Re,* and then the gradient drops when the flow rate approaches the turbulent region. A similar trend was obtained by Manawi et al. [24], when they varied both the feed and permeate flow rates simultaneously while keeping the flow rates equal. Ali et al. [23] showed that the permeate flux increases linearly against TPC values at low *Re* (until TPC = 0.84). Then, the permeate flux exponentially increases with TPC in the turbulent region. They stated that any small increment in TPC after their critical value of 0.84 would significantly increase the permeate flux. Though this statement is correct, it is evident from Fig. 9 that a massive change in the flow rate of the system is required to obtain any increment in the TPC values in the turbulent region. Hence, the water production gradient drops at higher *Re* values when it reaches turbulent flow as the flow rate is varied linearly in these experiments (Fig. 10a).

The permeate flux increases linearly with increasing the feed temperature (Fig. 10b). However, it has been commonly reported in the literature that the permeate flux exponentially increases when the feed temperature increases [36,37]. The discrepancy could be due to the shorter active membrane length used in the literature than what is used in this study. At the permeate side, moving from Points *D* to *A*, the surface temperature only increased by 2.2 °C when the feed temperature was 35 °C. However, the surface temperature increased by 19.2 °C when the feed temperature was set at 75 °C. The same trend was observed on the feed side. The considerable surface temperature loss along the membrane at high feed temperature directly affects the permeate flux. Hence, the permeate flux varies linearly rather than exponentially in these experiments. Though not common, few commercial membranes have shown a linear relationship [38,39] or a nearly linear relationship [40] between permeate flux and feed inlet temperature.

Preliminary results showed that the temperature readings change significantly when the system is not stable. Therefore, ample time was given for the system to stabilise before any measurements were recorded. Once stable, the temperature readings fluctuated around a given set of temperature readings for each measurement point (Fig. 11). For example, temperature readings recorded in experiment 55 °C_ 25 °C_0.3 L/min are shown in Fig. 11 for two Points *A* and *B* at the feed side. Point *A* is closest to the feed inlet and hence, has the highest fluctuations in temperature readings. Closer to the feed inlet, feed mixing is higher, and hence, the fluctuation becomes higher. Moving away from the feed inlet, Point *B*, has a steadier flow and, therefore, a lower fluctuation. A similar trend was also observed for the other operating conditions.

The temperature fluctuation increases as the flow rate is increased. As the flow becomes more turbulent, the mixing in the flow increases and results in higher fluctuations in temperature readings. However, in all cases, after the system has become stable, it would fluctuate around a given value. Therefore, a low flow rate (0.5 L/min) was chosen for the second set of experiments with varying feed temperatures. At this junction, it is appropriate to mention that the preliminary results showed that 55 °C and 25 °C for feed temperature and permeate temperature, respectively, were the best combination of temperatures to operate for the first set of experiments with varying flow rates. Fig. 7 shows that feed temperature below 55 °C resulted in very low TP effects, making any changes in temperature profile caused by flow rate changes

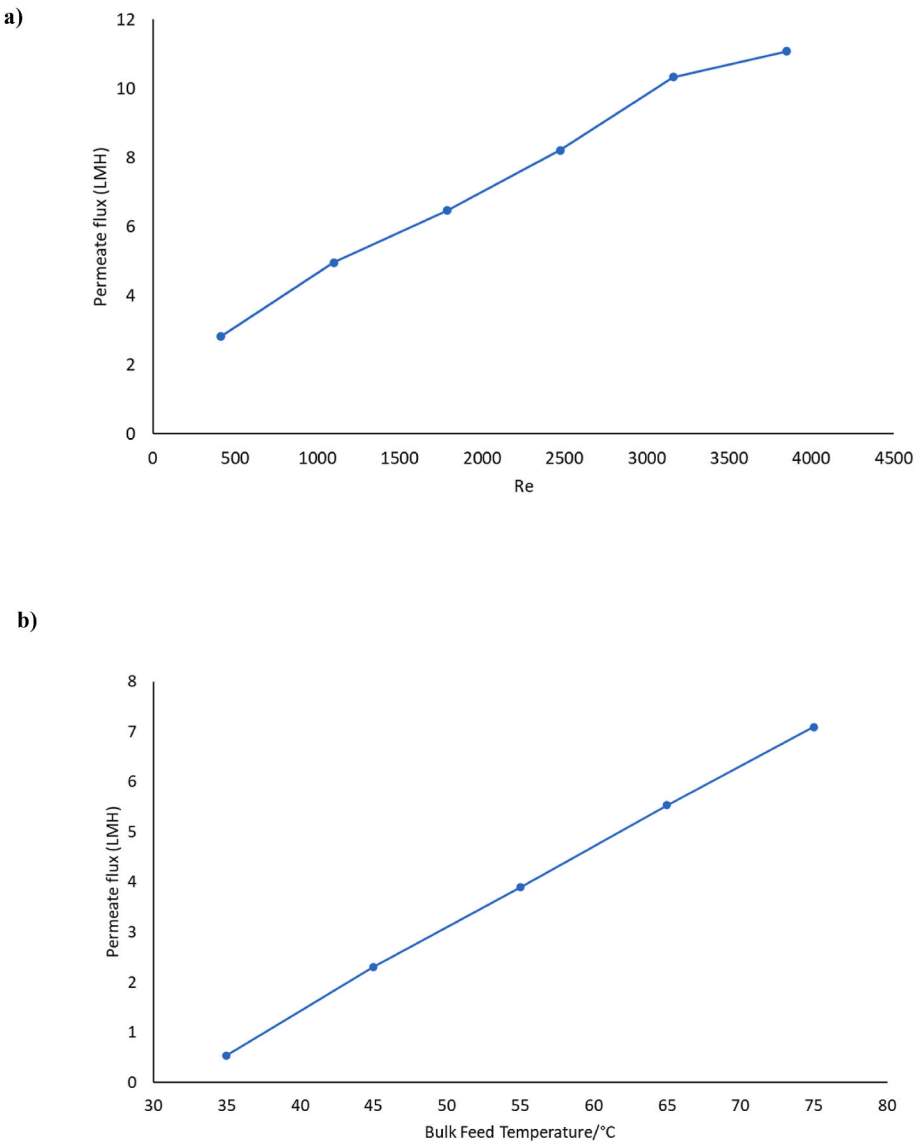

Fig. 10. **a**) The permeate flux at varying flow rates (0.3 L/min to 2.8 L/min (top). The feed temperature, permeate temperature and salinity were fixed at 55 °C, 25 °C and 3 g/L, respectively, and **b**) permeate flux at varying feed temperatures (35 °C–55 °C) (bottom). The permeate temperature, flow rate and salinity were fixed at 25 °C, 0.5 L/min, and 3 g/L respectively.

challenging to detect. However, feed temperatures above 55 °C will make the TP effects caused by the impacts of feed temperature more dominant than the impacts of the flow rates.

Although it has been established that feed temperature is the dominant factor that impacts the productivity (permeate flux) of the MD systems [24,41,42], this research indicates that the flow velocity and the flow pattern (membrane length) play a more critical role in determining the temperature profile along the membrane. Feed temperature significantly affects TP; however, the effects of varying the flow rate have a higher impact on the shape of the temperature profile (i.e., the extent of TP) (Figs. 5 and 7). Because the temperature has an exponential relationship with the vapour pressure (driving force) of the system, feed temperature changes will directly impact the system's productivity. In contrast, the flow rate indirectly impacts the productivity of the DCMD system. Flow rates influence the temperature profile along the membrane and the retention time of the flow which indirectly impacts the productivity of the system.

4. Conclusions

A custom-made DCMD cell was designed to analyse the temperature polarisation phenomena along the membrane for varying flow rates and feed temperatures. Using fundamental principles yet a unique approach, this research captures the temperature profile across and along the membrane for both feed and permeate sides using miniature thermocouples for the first time. The temperature profile directly relates to the extent of TP. The closest thermocouple was placed 0.3 mm perpendicular to the membrane, whose readings were considered the surface temperature of the membrane in this research. This research found that the TP is not linear perpendicular to the membrane (channel height), and the intensity of polarisation is the highest closest to the membrane ($Z/H < 0.4$). The inlet and outlet of both feed and permeate play a significant role in the extent of TP along the membrane than what was previously presumed or discussed in the literature. The inlet has a higher impact on the temperature profile than the outlet along the membrane.

The experimental results showed that temperature polarisation is sensitive and dominant at low *Re* numbers and high feed temperatures and is minimal at low-temperature differences across membranes

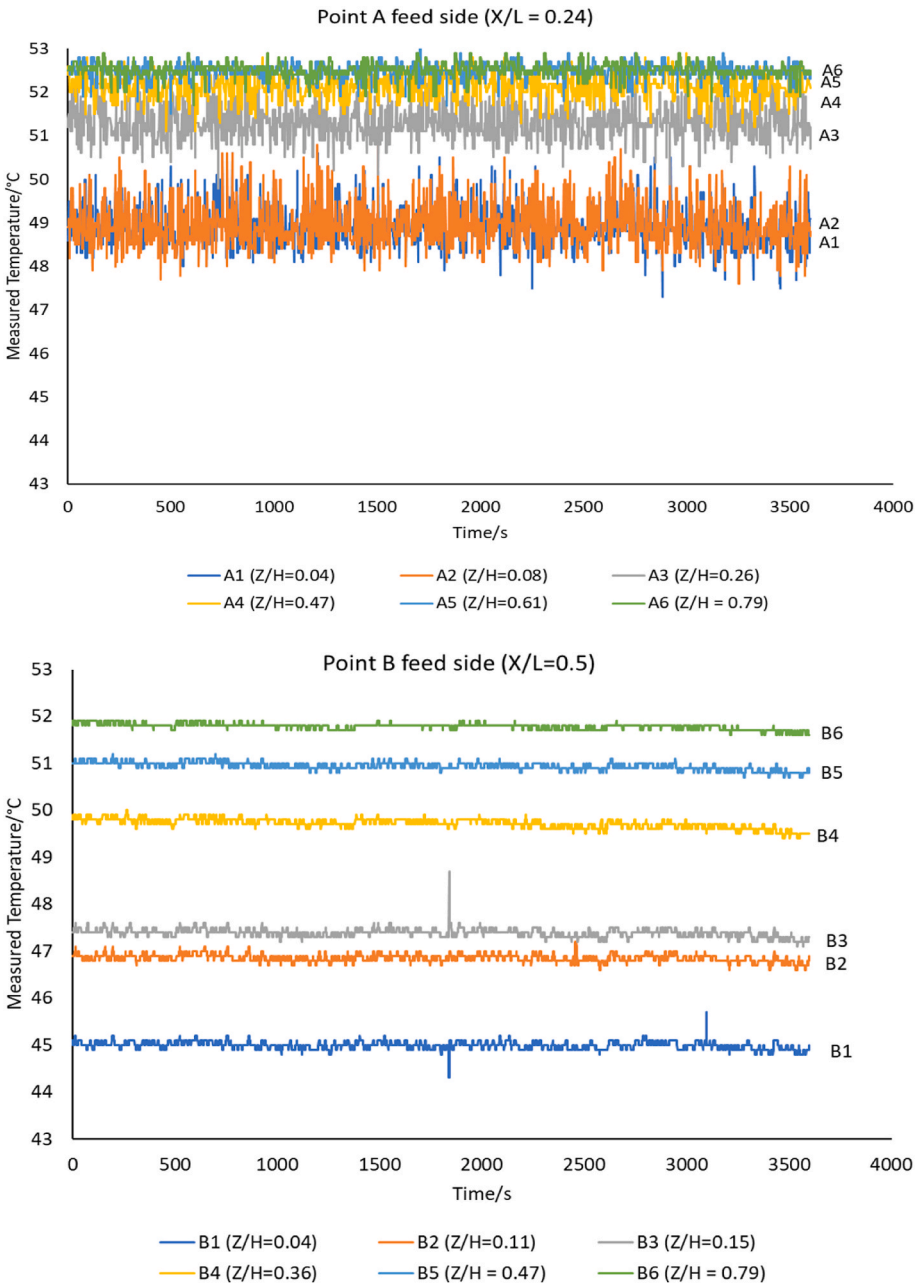

Fig. 11. The temperature variation recorded for 55 °C_ 25 °C_0.3 L/min for points A (top) and B (bottom) at the feed side for a period of 1 h.

operated at turbulent flow. This research shows that the widely used index, TPC, is an inadequate indicator to study TP phenomena along the membrane. However, it can be used to obtain a superficial understanding of the TP changes with varying operating conditions. There is almost a linear change in the surface temperature along the membrane away from the effects of the inlet and outlet. The change in surface temperature along the membrane (of length 422 mm) was notably greater at high feed temperatures (12.9 °C and 19.2 °C) than that at low feed temperatures (2.0 °C and 2.2 °C) for both feed and permeate sides, respectively. The monumental change (loss of driving force) at both feed and permeate sides for high feed temperatures resulted in a linear relationship between permeate flux and feed temperature in this research. This research also showed that although the feed temperature might be the dominant factor that influences the permeate flux by directly influencing the driving force of the system, the flow rates play a major role in the extent of TP.

Author statement

Hirad Ahamed Hijaz: Investigation, Methodology, Formal analysis, Visualization, Writing.
Masoumeh Zargar: Review & editing,
Abdellah Shafieian: Review & editing.
Amir RaZmjou: Review & editing.
Mehdi Khiadani: Supervision, Conceptualization, Review & editing.

Declaration of competing interest

We wish to confirm that there are no known conflicts of interest associated with this publication and there has been no significant financial support for this work that could have influenced its outcome.

Data availability

Data will be made available on request.

Acknowledgment

I would like to thank Memsift Innovation Singapore for gifting the membrane for this research. Our heartfelt gratitude goes towards Adrian Davis, our technical officer, for assisting in designing and manufacturing of the DCMD cell.

Appendix A. Supplementary data

Supplementary data to this article can be found online at https://doi.org/10.1016/j.memsci.2023.122089.

References

[1] M. Khayet, Solar desalination by membrane distillation: dispersion in energy consumption analysis and water production costs (a review), Desalination 308 (2013) 89–101, https://doi.org/10.1016/j.desal.2012.07.010.
[2] J. Wu, K.R. Zodrow, P.B. Szemraj, Q. Li, Photothermal nanocomposite membranes for direct solar membrane distillation, J. Mater. Chem. A 5 (45) (2017) 23712–23719, https://doi.org/10.1039/C7TA04555G.
[3] L. Chen, P. Xu, H. Wang, Interplay of the factors affecting water flux and salt rejection in membrane distillation: a state-of-the-art critical review, Water 12 (2020) 2841, https://doi.org/10.3390/w12102841.
[4] M.A.E.R. Abu-Zeid, Y. Zhang, H. Dong, L. Zhang, H.L. Chen, L. Hou, A comprehensive review of vacuum membrane distillation technique, Desalination 356 (2015) 1–14, https://doi.org/10.1016/j.desal.2014.10.033.
[5] A. Anvari, A. Azimi Yancheshme, K.M. Kekre, A. Ronen, State-of-the-art methods for overcoming temperature polarization in membrane distillation process: a review, J. Membr. Sci. 616 (2020), 118413, https://doi.org/10.1016/j.memsci.2020.118413.
[6] A. Ali, C.A. Quist-Jensen, F. Macedonio, E. Drioli, Optimization of module length for continuous direct contact membrane distillation process, Chem. Eng. Process: Process Intensif. 110 (2016) 188–200, https://doi.org/10.1016/j.cep.2016.10.014.
[7] R.W. Schofield, A.G. Fane, C.J.D. Fell, Heat and mass transfer in membrane distillation, J. Membr. Sci. 33 (3) (1987) 299–313, https://doi.org/10.1016/S0376-7388(00)80287-2.
[8] M. Qtaishat, T. Matsuura, B. Kruczek, M. Khayet, Heat and mass transfer analysis in direct contact membrane distillation, Desalination 219 (1) (2008) 272–292, https://doi.org/10.1016/j.desal.2007.05.019.
[9] A. Politano, G. Di Profio, E. Fontananova, V. Sanna, A. Cupolillo, E. Curcio, Overcoming temperature polarization in membrane distillation by thermoplasmonic effects activated by Ag nanofillers in polymeric membranes, Desalination 451 (2019) 192–199, https://doi.org/10.1016/j.desal.2018.03.006.
[10] A.S. Alsaadi, L. Francis, G.L. Amy, N. Ghaffour, Experimental and theoretical analyses of temperature polarization effect in vacuum membrane distillation, J. Membr. Sci. 471 (2014) 138–148, https://doi.org/10.1016/j.memsci.2014.08.005.
[11] S. Kalla, S. Upadhyaya, K. Singh, Principles and advancements of air gap membrane distillation, Rev. Chem. Eng. 35 (7) (2019) 817–859, https://doi.org/10.1515/revce-2017-0112.
[12] M. Khayet, P. Godino, J.I. Mengual, Theory and experiments on sweeping gas membrane distillation, J. Membr. Sci. 165 (2) (2000) 261–272, https://doi.org/10.1016/S0376-7388(99)00236-7.
[13] U.F. Alqsair, A.M. Alshwairekh, A.M. Alwatban, A. Oztekin, Computational study of sweeping gas membrane distillation process – flux performance and polarization characteristics, Desalination 485 (2020), 114444, https://doi.org/10.1016/j.desal.2020.114444.
[14] J. Zhang, J.-D. Li, M. Duke, M. Hoang, Z. Xie, A. Groth, C. Tun, S. Gray, Modelling of vacuum membrane distillation, J. Membr. Sci. 434 (2013) 1–9, https://doi.org/10.1016/j.memsci.2013.01.048.
[15] J.M. Rodríguez-Maroto, L. Martínez, Bulk and measured temperatures in direct contact membrane distillation, J. Membr. Sci. 250 (1) (2005) 141–149, https://doi.org/10.1016/j.memsci.2004.09.046.
[16] Y.M. Manawi, M.A.M.M. Khraisheh, A.K. Fard, F. Benyahia, S. Adham, A predictive model for the assessment of the temperature polarization effect in direct contact membrane distillation desalination of high salinity feed, Desalination 341 (2014) 38–49, https://doi.org/10.1016/j.desal.2014.02.028.
[17] P. Termpiyakul, R. Jiraratananon, S. Srisurichan, Heat and mass transfer characteristics of a direct contact membrane distillation process for desalination, Desalination 177 (1) (2005) 133–141, https://doi.org/10.1016/j.desal.2004.11.019.
[18] L. Chen, B. Wu, Research progress in computational fluid dynamics simulations of membrane distillation processes: a review, Membranes (2021).
[19] M.M.A. Shirazi, A. Kargari, A.F. Ismail, T. Matsuura, Computational Fluid Dynamic (CFD) opportunities applied to the membrane distillation process: state-of-the-art and perspectives, Desalination 377 (2016) 73–90, https://doi.org/10.1016/j.desal.2015.09.010.
[20] J. Lou, J. Vanneste, S.C. DeCaluwe, T.Y. Cath, N. Tilton, Computational fluid dynamics simulations of polarization phenomena in direct contact membrane distillation, J. Membr. Sci. 591 (2019), 117150, https://doi.org/10.1016/j.memsci.2019.05.074.
[21] A. Tamburini, P. Pitò, A. Cipollina, G. Micale, M. Ciofalo, A thermochromic Liquid crystals image analysis technique to investigate temperature polarization in spacer-filled channels for membrane distillation, J. Membr. Sci. 447 (2013) 260–273, https://doi.org/10.1016/j.memsci.2013.06.043.
[22] S. Santoro, I.M. Vidorreta, V. Sebastian, A. Moro, I.M. Coelhoso, C.A.M. Portugal, J. C. Lima, G. Desiderio, G. Lombardo, E. Drioli, R. Mallada, J.G. Crespo, A. Criscuoli, A. Figoli, A non-invasive optical method for mapping temperature polarization in direct contact membrane distillation, J. Membr. Sci. 536 (2017) 156–166, https://doi.org/10.1016/j.memsci.2017.05.001.
[23] A. Ali, F. Macedonio, E. Drioli, S. Aljlil, O.A. Alharbi, Experimental and theoretical evaluation of temperature polarization phenomenon in direct contact membrane distillation, Chem. Eng. Res. Des. 91 (10) (2013) 1966–1977, https://doi.org/10.1016/j.cherd.2013.06.030.
[24] Y.M. Manawi, M. Khraisheh, A.K. Fard, F. Benyahia, S. Adham, Effect of operational parameters on distillate flux in direct contact membrane distillation (DCMD): comparison between experimental and model predicted performance, Desalination 336 (2014) 110–120, https://doi.org/10.1016/j.desal.2014.01.003.
[25] Y.A. Çengel, J.M. Cimbala, M. Kanoğlu, Fluid mechanics: fundamentals and applications, in: SI Units, fourth ed., McGraw-Hill Education, 2020.
[26] B.R. Munson, T.H. Okiishi, W.W. Huebsch, Fluid Mechanics, seventh ed., Wiley New York, New York, 2013. SI Version.
[27] D.F. Elger, B.A. LeBret, C.T. Crowe, J.A. Roberson, Engineering Fluid Mechanics, twelfth ed., Wiley, Hoboken, NJ, 2019.
[28] T.L. Bergman, A.S. Lavine, F.P. Incropera, Fundamentals of Heat and Mass Transfer, seventh ed., John Wiley & Sons, Incorporated, 2011.
[29] T.Y. Cath, V.D. Adams, A.E. Childress, Experimental study of desalination using direct contact membrane distillation: a new approach to flux enhancement, J. Membr. Sci. 228 (1) (2004) 5–16, https://doi.org/10.1016/j.memsci.2003.09.006.
[30] K.W. Lawson, D.R. Lloyd, Membrane distillation, J. Membr. Sci. 124 (1) (1997) 1–25, https://doi.org/10.1016/S0376-7388(96)00236-0.
[31] A. Shafieian, M. Khiadani, A. Nosrati, Performance analysis of a thermal-driven tubular direct contact membrane distillation system, Appl. Therm. Eng. 159 (2019), 113887, https://doi.org/10.1016/j.applthermaleng.2019.113887.
[32] M. Hardikar, I. Marquez, T. Phakdon, A.E. Sáez, A. Achilli, Scale-up of membrane distillation systems using bench-scale data, Desalination 530 (2022), 115654, https://doi.org/10.1016/j.desal.2022.115654.
[33] M. Rabie, M.F. Elkady, A.H. El-Shazly, Effect of channel height on the overall performance of direct contact membrane distillation, Appl. Therm. Eng. 196 (2021), 117262, https://doi.org/10.1016/j.applthermaleng.2021.117262.
[34] J. Phattaranawik, R. Jiraratananon, A.G. Fane, Heat transport and membrane distillation coefficients in direct contact membrane distillation, J. Membr. Sci. 212 (2003) 177–193, https://doi.org/10.1016/S0376-7388(02)00498-2.
[35] M. Khayet, M.P. Godino, J.I. Mengual, Study of asymmetric polarization in direct contact membrane distillation, Separ. Sci. Technol. 39 (1) (2005) 125–147, https://doi.org/10.1081/SS-120027405.
[36] B.B. Ashoor, S. Mansour, A. Giwa, V. Dufour, S.W. Hasan, Principles and applications of direct contact membrane distillation (DCMD): a comprehensive review, Desalination 398 (2016) 222–246, https://doi.org/10.1016/j.desal.2016.07.043.
[37] M.S. El-Bourawi, Z. Ding, R. Ma, M. Khayet, A framework for better understanding membrane distillation separation process, J. Membr. Sci. 285 (1) (2006) 4–29, https://doi.org/10.1016/j.memsci.2006.08.002.
[38] P. Pal, A.K. Manna, Removal of arsenic from contaminated groundwater by solar-driven membrane distillation using three different commercial membranes, Water Res. 44 (19) (2010) 5750–5760, https://doi.org/10.1016/j.watres.2010.05.031.
[39] R.d.S. Silva, C.D.Á.K. Cavalcanti, R.d.C.S.C. Valle, R.A.F. Machado, C. Marangoni, Understanding the effects of operational conditions on the membrane distillation process applied to the recovery of water from textile effluents, Process Saf. Environ. Protect. 145 (2021) 285–292, https://doi.org/10.1016/j.psep.2020.08.022.
[40] S. Adnan, M. Hoang, H. Wang, Z. Xie, Commercial PTFE membranes for membrane distillation application: effect of microstructure and support material, Desalination 284 (2012) 297–308, https://doi.org/10.1016/j.desal.2011.09.015.
[41] S.G. Lovineh, M. Asghari, B. Rajaei, Numerical simulation and theoretical study on simultaneous effects of operating parameters in vacuum membrane distillation, Desalination 314 (2013) 59–66, https://doi.org/10.1016/j.desal.2013.01.005.
[42] A. Shafieian, M. Khiadani, A multipurpose desalination, cooling, and air-conditioning system powered by waste heat recovery from diesel exhaust fumes and cooling water, Case Stud. Therm. Eng. 21 (2020), 100702, https://doi.org/10.1016/j.csite.2020.100702.